Available online at www.sciencedirect.com

ScienceDirect

Energy Procedia 80 (2015) 131 – 140

Energy Procedia

12th Deep Sea Offshore Wind R&D Conference, EERA DeepWind'2015

Offshore Wind Farm Wake Effect on Stratification and Coastal Upwelling

Mostafa Bakhoday Paskyabi[a,b]

[a]Geophysical Institue, University of Bergen, Norway
[b]Bjerknes Center for Climate Research, Bergen, Norway

Abstract

In this study, the interactions between an offshore wind farm, upper-ocean currents, and stratification are examined under shallow water conditions from a two-dimensional modeling standpoint. The modeling results from two numerical simulation runs provide new insights on the formation of downwind vortex streets and the adjustment of coastal processes, such as upwelling and stratification. The distorted farm-induced wind deficits are calculated by the concept of single- and multiple-wake models. By assuming farm geometry as a large rigid rectangle, the numerical results of a shallow water model demonstrate the formation of vortex shedding wakes in the downwind of the wind farm. The slice model simulation runs, as the second numerical experiment, will address the coastal upwelling and geostrophic adjustment of density fronts in the presence of wind farm effects over a sloping bathymetry. We apply gravity wave effects using a wave-dependent aerodynamic roughness length when assuming the wind farm as an array of multiple turbines. Despite dynamical differences between simulation runs assuming farm as a rigid element and those considering farm as a cluster of single turbines, the results show some aspects of the farm-induced modulations on the pycnocline displacements and on the spatial-temporal evolution of the coastal upwelling. Although each simulation run has a unique scientific focus, the overall achieved numerical results are greatly able to improve the understanding of physical coupling between the wind farms and upper ocean dynamical processes.

© 2015 The Authors. Published by Elsevier Ltd. This is an open access article under the CC BY-NC-ND license (http://creativecommons.org/licenses/by-nc-nd/4.0/).
Peer-review under responsibility of SINTEF Energi AS

Keywords: Offshore wind farm; Coastal upwelling; Vortex street; Density frons; Shallow water equation; Wake model.

1. Introduction

Wind energy has been recognized as one of the important resources of green energy which meets the increasing electricity demands in a very sustainable manner. Additionally, offshore wind energy has gained more attention

1876-6102 © 2015 The Authors. Published by Elsevier Ltd. This is an open access article under the CC BY-NC-ND license (http://creativecommons.org/licenses/by-nc-nd/4.0/).
Peer-review under responsibility of SINTEF Energi AS
doi:10.1016/j.egypro.2015.11.415

due to its minimal impacts on the physical environment. However, deploying multiple-turbine arrays in the ocean necessitates the need for the assessment of the potential links between these large man-made structures and upper-ocean dynamical processes such as upper-ocean turbulent mixing, surface gravity waves, currents, local scour, local sediment variations, and (offshore and onshore) Ekman drifts in the offshore site districts.

While the effects of the offshore wind farms on the oceanographic processes have been addressed extensively during the recent years, a few research studies have been conducted to provide the detailed analysis of such local and far-field influences theoretically, numerically, and observationally. Lass et al. 2008 [1] conducted field measurements of acoustic backscattering and currents to study the pile-induced turbulence and mixing. Their measurements were carried out at the Western Bridge of the Great Belt Fixed Link, Denmark. The results suggested the plankton growth, turbulence energy levels, particles' settling rates, and particles' suspension time as being quantities which are influenced substantially by the large wind farm. Broström 2008 [2] investigated numerically the formation of coastal upwelling with speeds greater than 1 m/day for wind speeds ranging between 5 to 10 m s^{-1} in a large wind farm district. He showed that the pycnocline displacement increases directly as a function of wind farm characteristic length associated with the internal Rossby radius. Bakhoday-Paskyabi and Fer 2012 [3] studied the relationship between the strength of upwelling and the farm size by including contributions from the surface gravity waves. They showed that waves (particularly Stokes drifts) are able to increase the magnitude of the pycnocline displacements.

To reduce the existing uncertainty in the modeling of the farm-ocean interactions, we first investigate two empirical wake models which enable us to adequately predict the wake spatial distributions downwind of each single wind turbine (Section 2). The formation of the vortex streets in the lee side of a large wind farm is then studied using a two-dimensional shallow water model. The formed vortices can induce vibrations in a broad range of frequencies to the farm (Section 3.1 and 4). Another two-dimensional vertical ocean model is used to investigate the change in the structure of the coastal upwelling and stratification caused by the appearance of a large wind farm. In all numerical investigations, the farm is assumed either as a rigid body, or an array of multiple turbines (Section 3.2 and 4). The velocity deficits used are then calculated from a multiple-wake model.

2. Wind-farm interaction

The wake of a single turbine is generated due to the movements of turbine blades leading to changes in the wind field and the ambient turbulence intensity in the downwind areas. These changes reduce the output energy and increase the fatigue damages and loads imposed to each single turbine. Furthermore, due to the substantial distortion of wind field by the multiple wakes, the upper ocean model predictions in the farm sites will be directly linked to the quality of the wake modeling. In this section, we present two linearized wake models [4]: (1) Jensen wake model; and (2) Larsen wake model.

2.1. Jensen wake model

This model describes a single wake distribution by assuming that the wake's diameter is expanded linearly relative to the radial distance behind the turbine. Figure 1-a and b visualize a single Jensen's wake as a function of wake decay coefficient, which is controlled by the atmospheric turbulence intensity (note that both the turbulence intensity and the decay coefficient grow behind the turbine).

By assuming the conservation of momentum in the wake district, the wind speed at the downwind of the turbine is given by

$$v = v_\infty + v_\infty\left(\sqrt{1 - C_T} - 1\right)\left(\frac{R_0}{R(x)}\right)^2, \quad (1)$$

where v denotes the wind velocity at the downstream wake, v_∞ is the undisturbed wind velocity, R_0 is the turbine rotor radius, x is the radial distance (in the downwind area of the turbine) along the incoming wind direction, $R(x)$ is the wake diameter which is related to the diameter of the turbine via: $R(x) = R_0 + \beta x$, where β is a dimensionless constant called decay coefficient, and $C_T = \beta(1 - \beta)$ is the turbine thrust coefficient. Figure 1-a

and b illustrate the effects of a single turbine on the wake decay and wind deficit. The results corresponding to $\beta = 0.025$ gives slower growth of the wake diameter with different strength expansion than those of obtained for the case $\beta = 0.075$.

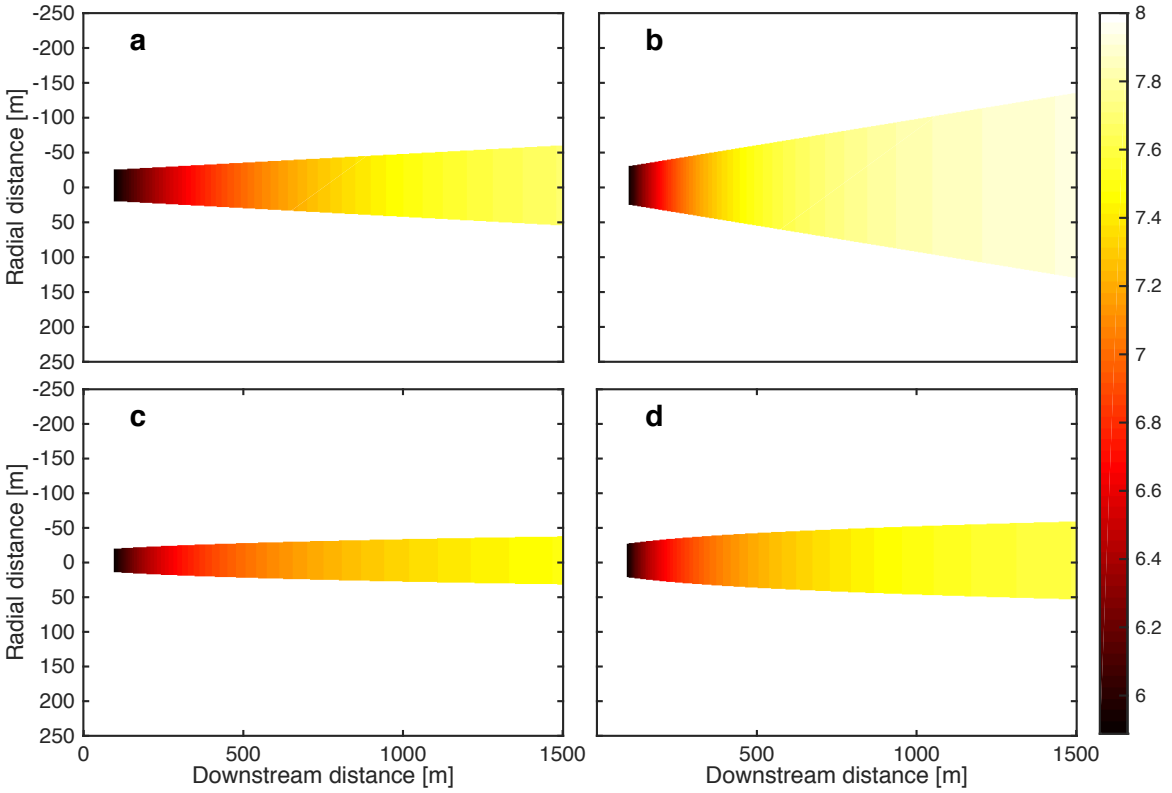

Fig. 1 Development of wake behind a wind turbine for the free stream wind speed of $v_\infty = 10$ m s^{-1}: (a) Jensen wake model for $\beta = 0.025$; (b) Jensen wake model for $\beta = 0.075$; (c) Larsen wake model for $I_u = 0.06$, where I_u denotes the turbulence intensity; and (d) Larsen wake model for $I_u = 0.12$. The rotor diameter in this simulation is set to 42 m, and wind blows from the west.

2.2. Larsen wake model

In this model, wake is assumed as an axisymmetric profile whose diameter grows non-linearly along the radial distance behind the wind turbine. To derive governing equations of Larsen wake model, the Prandtl's turbulent boundary layer is utilized under assumptions of an incompressible, stationary, and axisymmetric flow [6]. The actual form of this wake model is expressed by

$$v_\infty - v = -\frac{v_\infty}{9}\left(C_T A (x+\gamma)^{-2}\right)^{\frac{1}{3}}\left\{y^{\frac{3}{2}}(3c_1^2)C_T A (x+\gamma)^{-\frac{1}{2}} - \left(\frac{35}{2\pi}\right)^{\frac{3}{10}}(3c_1^2)^{-\frac{1}{5}}\right\}^2, \quad (2)$$

where c_1 is a non-dimensional mixing coefficient (dependent on the turbulence intensity), A denotes the rotor area, and γ is a variable depending on an effective rotor diameter. Figure 1-c and d show wake representations for a

wind turbine with ambient turbulence intensities of 0.06 and 0.12, respectively. The free stream wind speed is set to 10 m/s. It can be seen that the Larsen model is too sensitive to the ambient turbulence intensity, and the rate of the wake expansion is significantly lower for the turbulence intensity of 0.06 than that of for 0.12.

2.3. Wind profile

According to the similarity theory of Monin and Obukhov, the wind speed at the marine atmospheric boundary layer can be described through a log-linear profile [3]:

$$v(z) = \frac{v_{*a}}{\kappa}\left[\ln\left(\frac{z}{z_0}\right) - \phi_m\left(\frac{z}{L}\right)\right], \tag{3}$$

where v_{*a} is an air-side friction velocity, $\kappa = 0.41$ denotes the von Kármán constant, z_0 is an aerodynamic surface roughness length depending on wind conditions and sea-state, ϕ_m is a universal stability function, and L is the Monin-Obukhov length scale. If the wind velocity at the reference hub height is known, v_{hub}, the wind speed at any arbitrary height, z, (in the absence of the boundary layer stability effect, i.e. $\phi_m = 0$) can be derived using Eq. (3) from

$$v(z) = v_{hub}\frac{\ln(z/z_0)}{\ln(z_{hub}/z_0)}, \tag{4}$$

where z_{hub} denotes the hub height.

2.4. Surface gravity waves

In the presence of surface gravity waves, the total wind stress contains a wave-induced component. Assuming the total wind stress as a constant relative to the height, the aerodynamic roughness length (Eq. 3) under the influence of the surface gravity waves can be determined by a wave-dependent varying coefficient, α, through the Charnock relation [5,6]:

$$z_0 = \frac{\alpha v_{*a}^2}{g}, \tag{5}$$

where g is the gravitational acceleration, and in the presence of wave energy spectrum information, the Charnock parameter is determined through

$$\alpha = \frac{\alpha_v}{\sqrt{1-\frac{\tau_w}{\tau_a}}}, \tag{6}$$

where α_v=0.01 and τ_w is the wave-induced stress [5,6]. Neither Jensen nor Larsen models consider the vertical asymmetry resulting from the vertical wind shear and the surface gravity waves. In this study, we address the inclusion of gravity waves and the vertical shear effects using Eqs. (1,2,4,5) to generate cross-section wake pattern. The distribution of velocity deficit along *y*-axis is formulated using a Gaussian-type function. More details can be found in [3].

3. Ocean models

This section provides a brief overview of the shallow water equations and the two-dimensional vertical ocean model to study the wind farm interaction with upper-ocean density fronts and currents.

3.1. Two-dimensional shallow water equations

Under the assumption of the hydrostatic pressure, the Navier-Stokes equations are reduced to the shallow water equations as

$$\frac{\partial \boldsymbol{q}}{\partial t}+\frac{\partial \boldsymbol{F}}{\partial x}+\frac{\partial \boldsymbol{G}}{\partial y}=\boldsymbol{S}, \tag{7}$$

in which

$$\boldsymbol{q}=\begin{bmatrix} h \\ hu \\ hv \end{bmatrix},\quad \boldsymbol{F}=\begin{bmatrix} uh \\ hu^2+\frac{1}{2}gh^2 \\ uvh \end{bmatrix},\quad \boldsymbol{G}=\begin{bmatrix} hv \\ uvh \\ v^2h+\frac{1}{2}gh^2 \end{bmatrix},\qquad \boldsymbol{S}=\begin{bmatrix} 0 \\ f_{Cor}v-gb_x+\tau_x+S_f^x \\ -f_{Cor}u-gb_y+\tau_y+S_f^y \end{bmatrix}$$

where $z=-b(x,y)$ denotes the bathymetry, f_{Cor} is the Coriolis parameter, $h=-b+\eta$ is the water depth, where η indicates the surface elevation. $\boldsymbol{S_f}=\left(S_f^x,S_f^y\right)$ is the horizontal bed friction vector:

$$\boldsymbol{S_f}=c_f\boldsymbol{u}|\boldsymbol{u}|,$$

where $c_f=C^{-2}h^{-1}$ is the bed friction coefficient, C denotes the Chézy's coefficient with typical value of 37-40 $m^{1/2}s^{-1}$, and $\boldsymbol{\tau_x}=\left(\tau_x,\tau_y\right)$ is the horizontal wind stress. The detailed explanations for these equations can be found in [3].

3.2. Two-dimensional vertical ocean model

Let the upper ocean be occupied by a constant density layer with an initial thickness in *x*-*z* plane. The two-dimensional primitive equations of the flow geostrophic adjustment in the Cartesian coordinates are expressed as follows:

$$\frac{\partial u}{\partial t}+u\frac{\partial u}{\partial x}+w\frac{\partial u}{\partial z}-\overbrace{f_{Cor}}^{1}v=\overbrace{\frac{1}{\rho_0}}^{2}\frac{\partial P}{\partial x}+\overbrace{\frac{\partial(u'w')}{\partial z}}^{3}+\frac{\partial}{\partial z}\left(\overbrace{A_m}^{4}\frac{\partial u}{\partial x}\right),$$

$$\frac{\partial v}{\partial t}+u\frac{\partial v}{\partial x}+w\frac{\partial v}{\partial z}+f_{Cor}u=\frac{1}{\rho_0}\frac{\partial P}{\partial y}+\frac{\partial(v'w')}{\partial z}+\frac{\partial}{\partial z}\left(A_m\frac{\partial v}{\partial x}\right),$$

$$\frac{\partial \rho'}{\partial t}+u\frac{\partial \rho'}{\partial x}+w\frac{\partial \rho'}{\partial z}=\frac{\partial(\rho'w')}{\partial z}+\frac{\partial}{\partial z}\left(\overbrace{A_h}^{5}\frac{\partial \overbrace{\rho'}^{6}}{\partial x}\right),$$

$$\overbrace{\frac{\partial u}{\partial x}+\frac{\partial w}{\partial z}=0}^{7}$$

where term 1 denotes the Coriolis parameter ($=10^{-4}$), ρ' is the inverse of the reference density, term 3 indicates the vertical gradient of Reynolds stress, A_m and A_h (here $\sim 1\ m\ s^{-1}$) are the horizontal eddy viscosity and the horizontal eddy diffusivity, respectively. This model provides an approximation for three-dimensional ocean model as a result of excluding all gradients with respect to y, and gives a simple representation for the coastal upwelling and variability of stratification in the presence of the invariant surface forcing (see also [3]).

4. Results

The flow characteristics past a wind turbine and generally wake dynamics have essential impacts on the design and operation of offshore energy devices. Vortex streets can be one of such dynamical processes occurring in the downwind flow of single monopile or rigid large wind farm. Figure 2 shows the formation of vortex shedding behind a large wind farm as either a pair of counter-rotating vortices trapped in the lee of the farm, or a train of vortices extending far downwind. This process may cause oscillatory lift and drag forces resulting in vortex-induced vibrations to each individual turbine. Depending on the size of the offshore structures, monopile's diameter, wind farm characteristic length, the elasticity features of the platforms, the nature of cross-street and along-street spacing of the vortices, the wind forcing scales, and atmosphere stability conditions, these vortex-induced vibrations may exert a great amount of loads and fatigue damages to the platform. This makes the detailed knowledge about vortex formation and evolution an important determining factor in the design of the wind parks. Another important aspect of the formed vortex streets is their ability to generate farm-induced waves that can steepen and break up in the lee side of structures.

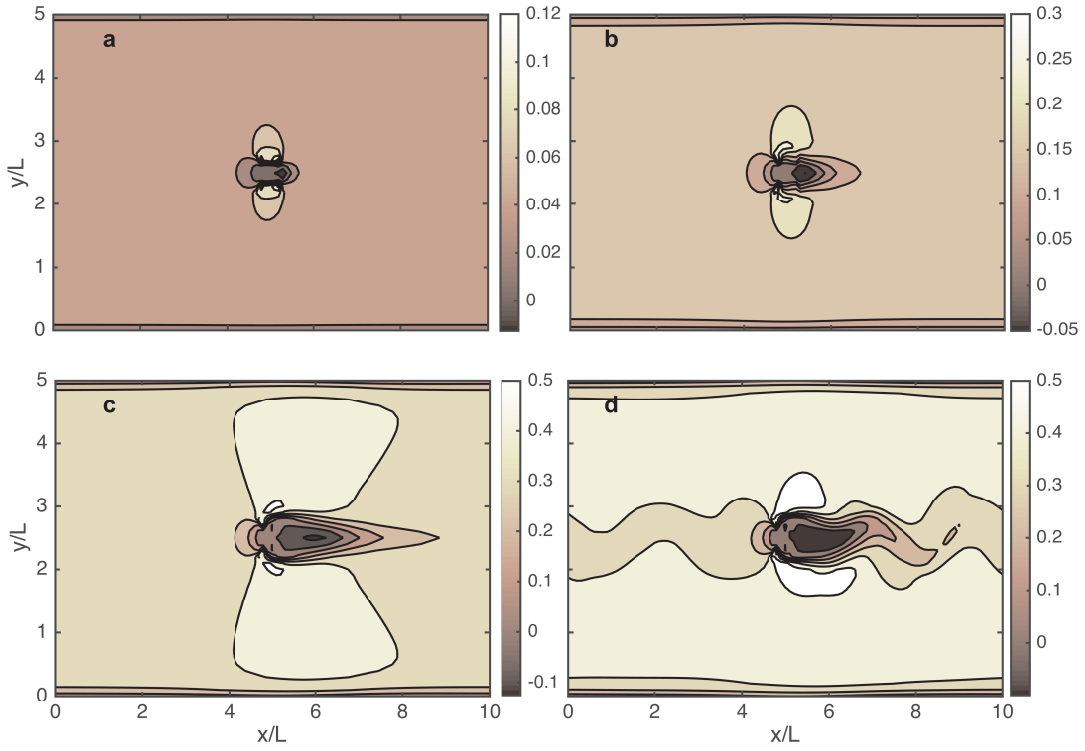

Fig. 2 The time evolution of wake formation after: (a) 12 hours; (b) 2 days; (c) 3 days; and (d) 5 days. In this example a large wind farm is treated as an island, and results represent very extreme and idealized situations for generation of such turbulent mechanisms.

Results in Fig. 2 have been produced using vertically integrated two-dimensional shallow water equations (Section 3.1). The U-component of vertically integrated current illustrates the local drops and subsidence events together with pressure gradients, which push flow around the wind park. The extension of these pressure gradients under the influences of wind forcing and farm characteristic size will result in the formation of vortex streets in the farm wake district. It should also be mentioned that although assuming farm as a rigid oscillating body (like an

elastic island) cannot properly describe the wake and vortex street behaviors, this idealized investigation can provide significant insights into such poorly understood phenomenon for the offshore wind energy technologies.

Simple analytical models, such as Jensen and Larsen wake models, are commonly used for representing wake physics due to their simplicity and little required computational efforts. In Fig. 3, the total wind field behind a cluster of 12 single turbines is illustrated using the wake overlapping technique and local superposition of the turbine-generated deficits [4]. This figure shows the simulated wake deficits for westerly free stream wind speed of 10 m s^{-1} and wake spreading factor of 0.03, required in the Jensen wake model. There exists an uncertainty corresponding to the change of the wind direction that has not been included in this simulation. This example demonstrates the importance of choosing appropriate wake model which is crucial for: (1) wind farm layout optimization; (2) site assessment; and (3) improvement of farm-ocean and farm-atmosphere interactions in the computational fluid dynamic codes. Furthermore, we address the existing gap between the ocean circulation models and the parameterization of wake, by replacing the wake parameterization (as used in [2] and [3]) by more optimal analytical representations. It is worth mentioning that the replacement of the following wind farm configuration (consisting of 12 single turbines) by a rigid solid body leads to an approximately 1 m s^{-1} difference in the prediction of the wake deficit for the same wind speed (i.e. 10 m s^{-1}, not shown).

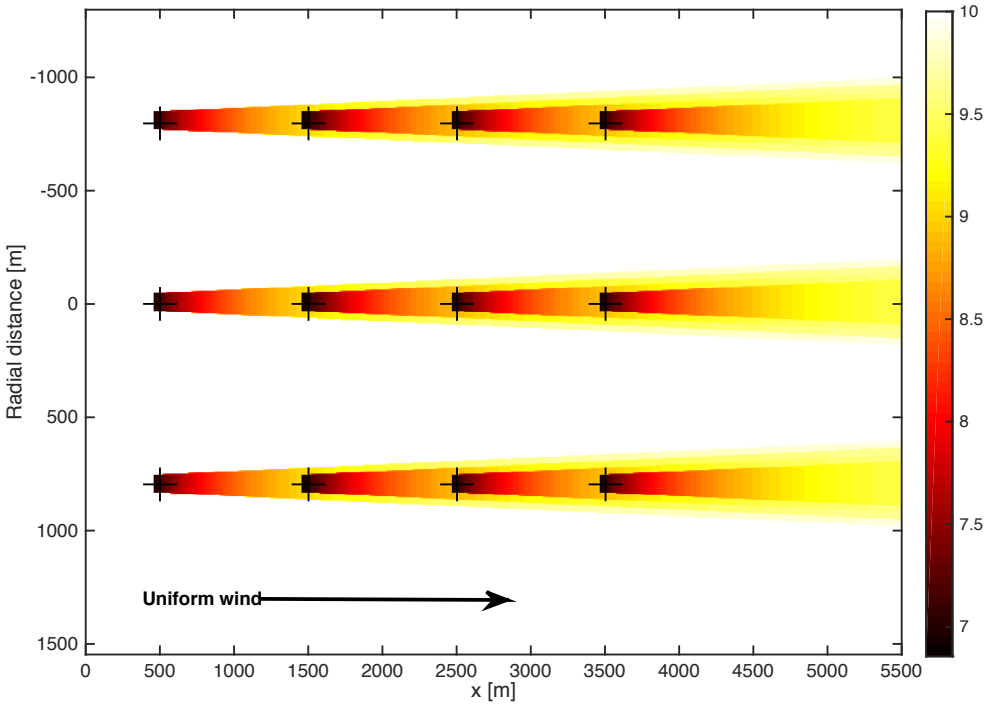

Fig. 3 Results of Larsen wake model for a wind farm including 12 turbines with rotor diameter of 84 m, horizontal separation of 1 km, and vertical separation distance of 800 m. Free stream wind sets to 10 m s^{-1}. We use the value of 0.04 for the decay coefficient.

In the previous examples, we investigated some aspects of wind farm wake and farm-generated vortex streets as important processes that influence the mutual interactions between the offshore wind farm and upper ocean processes. Another important physical process related to the coupled farm-ocean dynamics is the upper-ocean vertical current variability, i.e. upwelling and downwelling in the coastal regions.

Coastal upwelling regulates several physical processes in the surface boundary layer by forming some of the most productive ecological regions in the world's oceans. This process controls the light climatology of upper ocean, the transportation of planktonic organisms all the way through the mixed layer, the enrichment of ecosystem productivity, and the enhancement of air-sea chemical exchanges among many other aspects. Here, we try to present a more complete understanding of the interactions between topography, large wind farm, and the strong advective upwelling phenomenon. In Figs. 4 and 5, we illustrate a cross-section view of v-component of current and density anomalies in a sloping bathymetry using a two-dimensional vertical ocean model (Section 3.2). The simulation domain comprises of maximum water depth of 50 m, which decreases to 25 m along the x-axis. The grid spacing along x and z axes is set to 500 m and 5 m, respectively. We use open boundary for offshore lateral boundary, and the sea surface is forced by an alongshore wind stress (free stream wind speed of 10 m s^{-1} in the direction normal to the x-z plane). The surface mixed layer has an initial thickness of 10 m corresponding to a density of 1025 kg/m^3, which increases linearly beneath the pycnocline. We assume that horizontal eddy diffusivity and eddy viscousity are equal for this simulation (i. e. 7.5×10^{-2}). For the wake estimate, we use the Jensen wake model for a large wind farm with a characteristic length of $L = 5$ km as a rigid body (Fig. 4-b). The wind farm consists of 5 single turbines with 1 km separation distance centered at 50 km (Fig. 4-c). Furthermore, the surface gravity wave effects are accounted by the use of the aerodynamic roughness length (Eqs. 4-6). We use a bulk flux formulae to estimate westerly wind stress [6].

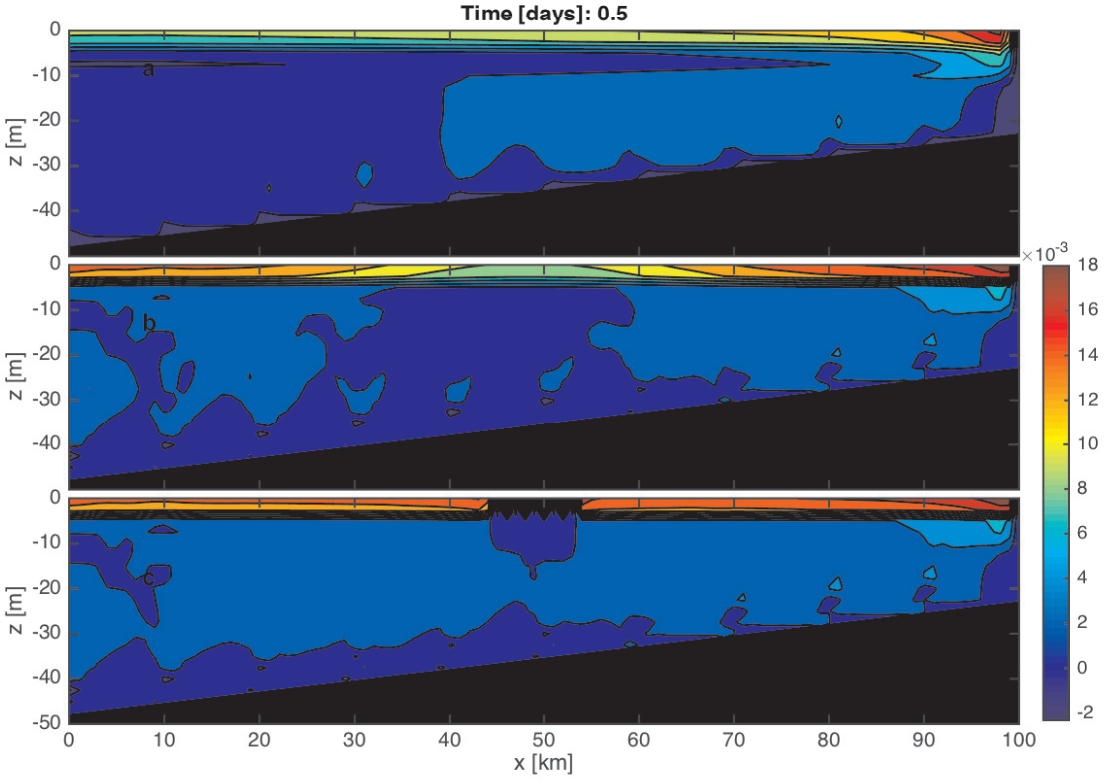

Fig. 4 Distribution of v-component of ocean current after 12 hours of simulation. (a) Run with no farm effect; (b) run under the influence of wind farm considered as a rigid body. The wind distribution is then parameterized by combining the Jensen wake model with an exponential distribution along the y-axis; (c) run in the presence of a cluster of 5 single turbines aligned along the y-axis with separation distance of 800 m. We use the same configuration for the wake model as used in Fig. 3.

Figure 4 shows the onset of Ekman drift formation at both surface and bottom boundary layers as a result of an

alongshore wind stress. In simulation with no farm effect (Fig. 4-a), a creeping onshore Ekman drift in the frictional bottom boundary layer moves the currents towards the coast with very high speed. Simultaneously, an offshore Ekman drift pushes surface layer towards the offshore in response to the wind forcing. Perturbations of the wind field, induced by accounting the wind farm effect, change the patterns of surface and bottom geostrophic flows due to the modulation of Ekman drifts at both boundary layers (Fig. 4-b and c). Furthermore, the inclusion of wind farm effects amplifies the sea-level gradients at the farm district.

Figure 5 displays the model simulation results for the density stratification (density anomaly relative to 1025 kg m^{-3}) and pycnocline spatial-temporal variations for: (1) no farm effect (Fig. 5-a); (2) farm effect for a farm considered as a rigid large body (L=5 km, Fig. 5-b); and (3) farm effect in which the farm consists of 5 separated single turbines. The density anomaly structures in these three runs imply that the created Ekman drift at the sea surface translates the farm-induced perturbation to the water column resulting in displacements of lateral flow and pycnocline oscillation. In the presence of the wind farm, the model anticipates a shorter distance between the coast and the density outcrop compared with the simulation run in the absence of farm effect. This can be explained by the farm-modified radius of Rossby deformation [3].

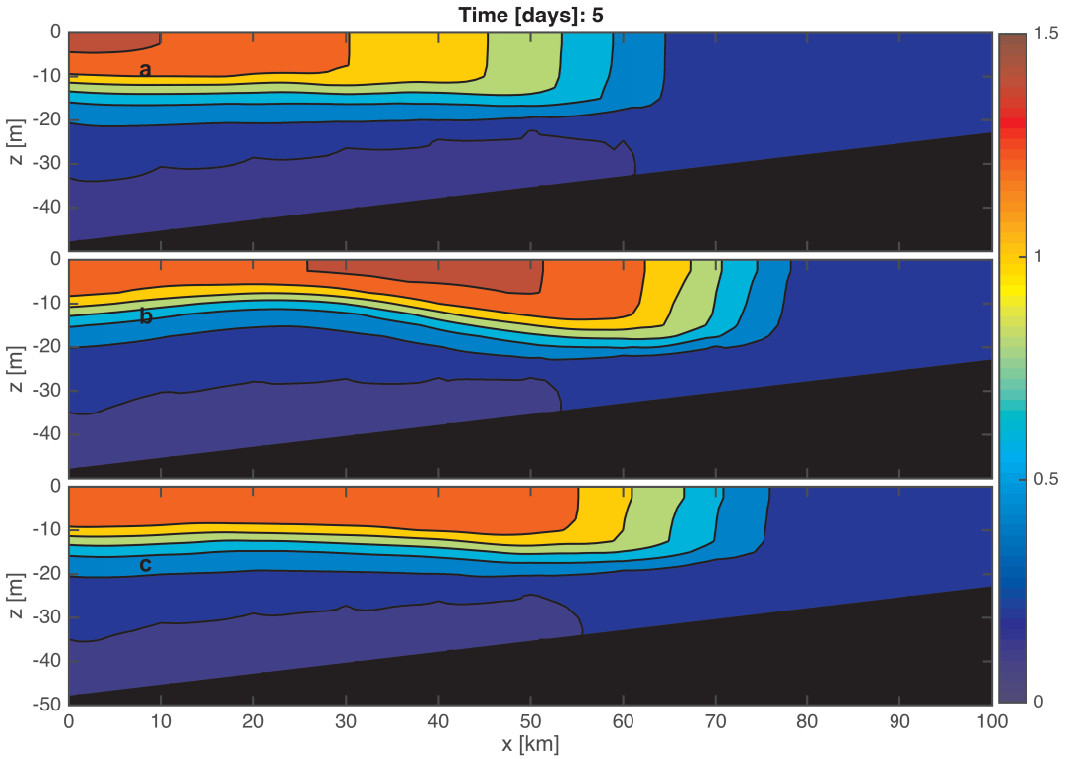

Fig. 5 Distributions of density anomaly after 5 days of simulation. (a) Run with no farm effect; (b) run in the presence of farm; and (c) run under the influence of a cluster of 5 turbines.

5. Conclusions

Due to large demands for the efficient development of renewable energy resources such as wind energy, offshore wind industries are gaining widespread attention, investments, and investigations among other types of reliable renewables. To make this energy more feasible, less expensive, and more popular, we need a comprehensive understanding of various underlying physics and important interacting mechanisms such as wind and wave interaction in the offshore farm districts. In this study, we ideally parameterized the excitation of wind field in the farm-located area accompanied with a significant reduction of wind stress in the downstream direction using a semi-experimental wake model. The interactions between the farm-generated disturbances in the wind field and in the upper-ocean physical processes were investigated from two idealized numerical simulation runs. Results suggested that the continuation of wind forcing and its interaction with offshore wind farms are able to generate and enhance the pressure gradient around the farm such that in the extreme case, vortex streets together with overturning flow will form on the farm wake regions. In the vertical ocean model run, we showed numerically that the farm-induced disturbances to the wind field can modulate the upwelling processes and change the upper ocean stratification pattern.

Acknowledgements

This work has been performed as part of the Norwegian Center for Offshore Wind Energy (NORCOWE) funded by the Research Council of Norway (RCN 1938211560) and partly by the OBLO (Offshore Boundary Layer Observatory) project (RCN: 227777).

References

[1] Lass HU, Mohrholz V, Knoll M, Prandke H. Enhanced Mixing Downstream of a Pile in an Estuarine Flow. J. Mar. Syst., 2008, 74, 505–527.
[2] Broström G. On the influence of large wind farms on the upper ocean circulation, Journal of Marine Systems, 2008,74, 585-591.
[3] Bakhoday-Paskyabi M, Fer I. Upper Ocean Response to Large Wind Farm Effect in the Presence of Surface Gravity Waves, Energy Procedia, 2012, 24, 245-254.
[4] Barthelmie RJ, Folkerts L, Larsen GC, Rados K, Pryor SC, Frandsen ST, Lange B, Schepers G. Comparison of wake model simulations with offshore wind turbine wake profiles measured by sodar, J. Atmos. and oceanic tech., 2006, 23.
[5] Bakhoday-Paskyabi M, Flügge M, Edson JB, Reuder J. Wave-induced characteristics of atmospheric turbulence flux measurements. Energy Procedia, 2013, 25, 102-112.
[6] Bakhoday-Paskyabi M, Fer I, Jenkins AD. Surface gravity wave effects on the upper ocean boundary layer: modification of a one-dimensional vertical mixing model, Cont. Shelf Res., 2012, 38, 63-78.